batteries

MDPI

Article

Lifecycle Evaluation of Lithium-Ion Batteries Under Fast Charging and Discharging Conditions

Olivia Bruj and Adrian Calborean *

National Institute for Research and Development of Isotopic and Molecular Technologies, 67-103 Donath, 400293 Cluj-Napoca, Romania; olivia.bruj@itim-cj.ro
* Correspondence: adrian.calborean@itim-cj.ro

Abstract: By employing electrochemical impedance spectroscopy, we performed an impedance analysis of three commercial Li-ion Panasonic NCR18650B cells in order to investigate the direct effects of their internal impedance on the operating voltage, rate capability, and efficiency and their practical capacity. We aimed to assess their performance, safety, and longevity when distinct fast charge/discharge rates were applied. By maintaining a constant fast discharge rate of 2C, we monitored the degradation speed and the influence of the C-rates on the LIBs by applying distinct charge rates, namely, 1C, 1.5C, and 2C. In order to understand how their performance correlates with usage conditions, an SoH evolution analysis, together with a Q–Q_0 total charge and energy consumption examination, was performed, taking into account that cycling monitoring is vital for ensuring their longevity and/or safety. Increasing the I_{charge} from 1C to 1.5C reduces the battery lifetime by ~50%, while in the case of fast charge/discharge rates of 2C, the lifetime performance decrease is almost ~70% due to a capacity loss that accelerates quickly when the charge rates increase. Moreover, for the latter cell, the last discharge rate can only go up to ~80% SoH, as the battery charge rate can no longer support faster degradation. In agreement with these results, the fluctuations in the Q–Q_0 total charge become more pronounced, clearly affecting LIB efficiency. High charge rates add an additional high voltage that increases the batteries' stress, leading to a shorter lifetime. Energy consumption data follow the same trend, in which efficiency decreases dramatically when losses appear because the internal resistance causes more and more heat to be produced during both fast charging and discharging.

Keywords: lithium-ion cells; lifecycle prediction; electrochemical impedance spectroscoy

Academic Editors: Mei Luo and George Zheng Chen

Received: 27 December 2024
Revised: 27 January 2025
Accepted: 1 February 2025
Published: 7 February 2025

Citation: Bruj, O.; Calborean, A. Lifecycle Evaluation of Lithium-Ion Batteries Under Fast Charging and Discharging Conditions. *Batteries* **2025**, *11*, 65. https://doi.org/10.3390/batteries11020065

1. Introduction

Lithium-ion cells have evolved rapidly in the last decades, becoming the backbone of the rechargeable energy store. They are currently the most attractive products for manufacturers worldwide due to their easy customizable technology. We refer here to the tremendous potential for modifying features like the cathode chemistry [1,2] and/or the cell format [3], which allows their features to be continuously improved in terms of high energy density [4], lifespan [5], light weight [6], good long-term performance [7], low self-discharge [8], fast charge times [9], temperature tolerance [10], etc. Providing a strong combination of these unique properties, lithium-ion cells have revolutionized the manner in which we power our portable electronic devices, electric vehicles (Evs), hybrid electrical vehicles (HEVs), and energy storage systems. When compared to traditional batteries, they are highly superior in terms of leakage resistance under environmental variations due to organic electrolytes that have a solidifying point much lower than that of

aqueous solution electrolytes, thus offering better operation capabilities at a wide range of temperatures [11–13].

The vast amount of research in the field has brought significant refinements to lithium batteries. The most common types include the following: (i) lithium iron phosphate (LFP) [14], in which the energy is stored separately from its discharging sequence by using a lightweight $LiFePO_4$ as a charge carrier; (ii) lithium cobalt oxide (LCO) [15], which incorporates layered LCOs in the positive electrode; (iii) lithium manganese oxide (LMO) [16], in which manganese dioxide is inserted into the cathode under different layers of $LiMnO_2$, $LiMnO_3$, Li_2MnO_2, and spinel $LiMn_2O_4$ or is integrated in different forms; (iv) lithium nickel manganese cobalt oxide (NMC) [17–21], in which metal oxides of lithium, nickel, manganese, and cobalt are mixed; (v) lithium nickel cobalt aluminum oxide (NCA) [22], which are used as the active materials at the positive pole by mixing several chemical elements such as nickel, cobalt, and aluminum; (vi) lithium titanate and lithium titanate oxide (LTO) [23], which are used as nanocrystals on the anode surface instead of graphite; (vii) lithium-sulfur (Li-S) [24] type, which involves lithium dissolution from the anode surface during discharge and reverse lithium plating to the anode while charging, etc.

Within all these technological developments, an accurate prediction and/or estimation of the state of health (SoH) is of tremendous importance not only for extending the batteries' lifetime [25] but also in terms of monitoring downtime in battery management systems [26]. This parameter is crucial for assessing the performance, safety, and longevity of lithium-ion batteries (LIBs), and thus, several methods have been used to estimate the SoH. Here, we name some of the most important methods: (a) voltage-based methods, implying an open circuit voltage (OCV) vs. a state of charge (SOC) relationship [27] or the voltage relaxation approach [28]; (b) impedance spectroscopy by electrochemical impedance spectroscopy (EIS) [29] or AC impedance [30]; (c) coulomb counting [31]; (d) machine learning methods with supervised learning [32] and deep learning [33]; (e) Kalman filtering [34]; (f) capacity estimation methods by cycle life modeling [35] and capacity fade models [36]; (g) data-driven models through regression analysis [37] and a random forest approach [38]; (e) thermal analysis [39]; state of charge (SoC) and state of health (SoH) coupling [40]; (h) modeling based on electrochemical principles using equivalent circuit models (ECM) [41] or the Thevenin [42], Randles [43], and pseudo-2D models [44]. An interesting theoretical approach that can be applied to LIB electronic analysis was developed by Máthé et al. [45,46], in which the electrical transport properties can be simulated within cell conditions.

In this context, we employed the electrochemical impedance spectroscopy (EIS) methodology [47–50] to study three commercial Panasonic lithium-ion cells in order to determine their lifetime performance when distinct fast charge/discharge rates were imposed. Applying this powerful diagnostic tool to LIBs to evaluate their performance [51], state of health (SoH) [52], and degradation mechanisms [53], we aimed to evaluate different approaches to the interpretation and validation of impedance measurements. In the particular context of lithium-ion cells, impedance reflects how the battery resists electrical current flow under alternating current (AC) conditions [54].

Therefore, by characterizing impedance in defining battery operational boundaries, we can estimate the performance and track the state of health (SoH) of our LIBs. It is known that Li-ion batteries excel in fast charge and discharge conditions, as they can absorb and release energy very fast. We therefore focus on investigating how much fast charging decreases battery efficiency over time and reduces energy storage due to the unused capacity. Energy consumption is also investigated, taking into account some key factors that can contribute to energy fluctuations in terms of different charge and discharge rates. By applying

fast charge rates, we try to understand when temporary voltage fluctuations appear (in which the battery may not absorb energy consistently, leading to thermal build up and internal resistance changes), and similarly, by fast discharging, how the energy output can fluctuate because the battery struggles to supply energy at a high rate, causing voltage sag. Understanding and controlling these factors can further improve the performance and longevity of LIBs, making them more reliable for a wide range of applications.

The current literature on EIS methodology used for the determination of a range of aging effects on lithium cells is extremely vast, and we have observed in many cases that the results can be significantly affected by the battery equivalent model employed to analyze the elements [55–58]. In the process of optimizing parameters derived from a Nyquist diagram, there is a strong need for intensive processing and good initial estimation, which might be very difficult to acquire. Moreover, precise EIS measurements demand expensive facilities, long cycling procedures, and algorithms with high-computational efforts, which make them nearly unsuitable for on-board systems. As these restrictions clearly limit the EIS technique, we aimed here to find reliable and fast methods through EIS technology without using Randle equivalent circuit models with their parameter estimation. We refer here to SoH parameter analysis, Q–Q_0 total charge parameters, or the energy consumption at fast charge and discharge rates. It is known that the available energy is the total energy released when the discharge is set at the lower voltage limit. This establishes a relationship between the remaining capacity and the time of use. The available capacity stored in the battery depends on the ambient temperature, the current, and the running conditions. As such, the current study encompasses distinct but related approaches that are capable of highlighting new diagnostic tools for aging prediction in lithium-ion cells. By keeping a constant fast discharge rate of 2C, we monitor the degradation speed and the influence of the C-rates on the LIBs by applying distinct charge rates, namely, 1C, 1.5C, and 2C. The dynamics of the lithium transport process is assessed, as well as its dependence on the charge rate with the aim of understanding how their performance correlates with usage conditions. The aim is to provide some reliable references for lithium-ion cell management, diagnose performance issues, and understand degradation mechanisms that depend on the charge/discharge rate variations, taking into account that cycling monitoring is vital for ensuring the longevity and/or safety of these cells.

2. Materials

2.1. Commercial Lithium-Ion Cells

Three lithium-ion NCR18650B-type batteries, produced by Panasonic, were purchased from the market and used in this study. Currently, they are the 18650-type battery with the highest (real) capacity, and due to their superior quality, they are mainly used in newer LED flashlights but also as part of the assembly of various other devices, such as power banks (external batteries), jump starters (car starting robots), hoverboards, and electric scooters and bicycles [59,60]. Moreover, it should be mentioned that these batteries were previously used in the Tesla model S (the first model) electric vehicle, which was of great interest at that time [61,62]. In Table 1, the most important battery specifications are described.

2.2. Experimental Setup

The VSP electrical laboratory equipment of BioLogic [63] was employed for impedance acquisition within all measurements. This system consists of a single computer board associated with four potentiostat channel boards, which make the VSP a very versatile multichannel potentiostat. A modular booster unit module of 100 A was used, and all the data were acquired, processed, and analyzed through EC-Lab software (version v11.61).

In Figure 1, the setup prepared for the LIB measurements is shown, in which the cells are connected to the VSP cables through crocodile clips.

Table 1. NCR18650B battery features.

Technical specifications		Dimensions	
Rated capacity at 25 °C	3200 mAh	Length	65.3 mm
Nominal capacity at 25 °C	Min. −3250 mAh	Diameter	18.5 mm
	Typ. 3350 mAh	Weight	47.5 g
Nominal voltage	3.6 V	Packaging: industrial bulk (for industrial use)	
Charging method	CC–CV		
Charging current	1625 mA		
Charging voltage	4.2 V		
Charging time	4 h		
Energy density	676 Wh/L		
Cathode material	Nickel oxide		

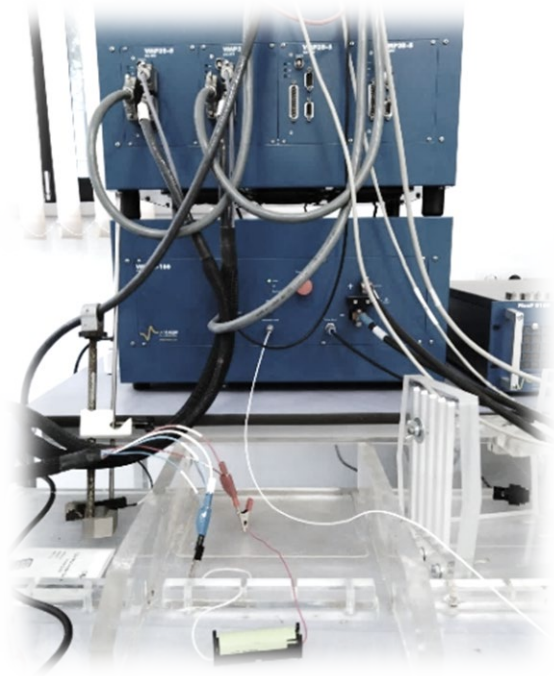

Figure 1. The experimental setup for PEIS acquisition.

The PEIS experiment was employed, performing impedance measurements in potentiostatic mode. We registered the frequency-dependent impedance, with a particular focus on monitoring the variation in imaginary impedance values against the frequency oscillations. As such, we evaluated the heterogeneous charge-transfer parameters with high precision. Figure 2 shows the PEIS general diagram, in which the potential of the working electrode follows the equation below [64]:

$$E_{we} = E + V_a \sin(2\pi f t) \quad (1)$$

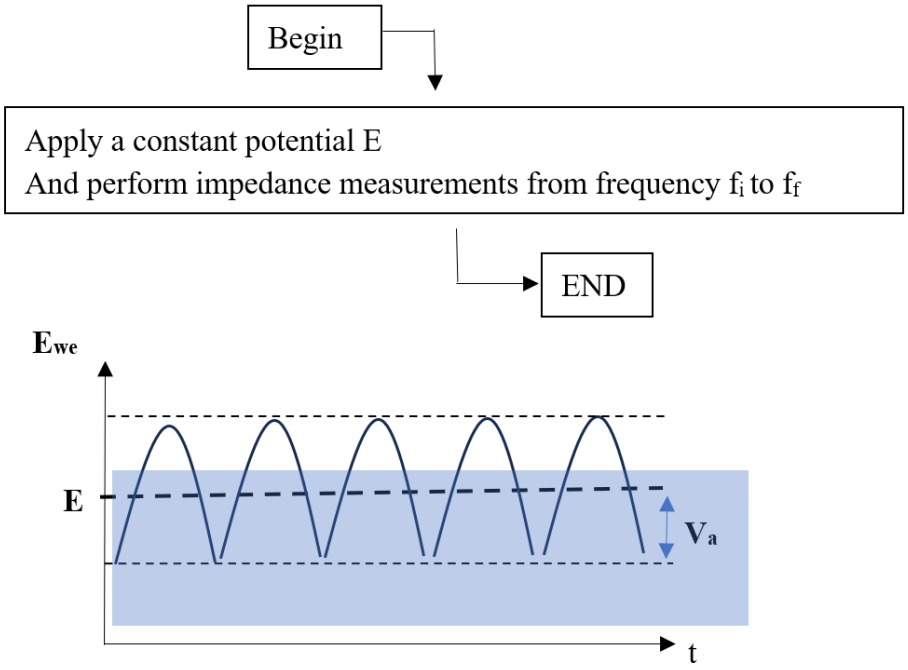

Figure 2. PEIS general diagram.

2.3. Electrochemical Impedance Spectroscopy (EIS)

The non-invasive electrochemical impedance spectroscopy (EIS) technique was used in different configurations of charge/discharge rates, offering important information about the physical–chemical processes that occur at both electrodes of lithium-ion batteries with their distinct impacts on degradation speed. Their lifetime performance and aging mechanisms were analyzed by tracking the changes in internal resistance and charge-transfer impedance, and then, the data were correlated with the SoH. The differences in impedance profiles during charging versus discharging were interpreted in terms of the LIB degradation phenomena, as it is known that impedance usually increases as a function of cell aging due to the degradation of the electrode materials, electrolytes, and electrical contacts within the cell. Thus, we gathered in a simple manner EIS data on Li battery charging rates in order to provide the optimal link between the SoH and battery lifetime predictions.

The overlapping processes across timescales were separated and interpreted, thus offering invaluable data for improving performance and longevity. In particular, we focused on the charge and discharge processes of LIBs, monitoring the impedance fluctuations that appear due to the shifts in the state of charge (SoC). Insights into key physical and electrochemical phenomena during these processes were discussed, thus aiming to refine the current densities and voltage limits in order to minimize resistive losses and improve cycling stability. However, performing EIS during active charging or discharging requires precise control to avoid interference from DC signals.

All the EIS measurements were performed in a temperature-controlled room, in which the temperature was set to 21 degrees throughout the study period (several months of cycling). We are fully aware of the impact of temperature effects on lithium-ion batteries, in which the electrochemical reactions that govern the cell performance are susceptible to temperature variations, but the scope of this paper is different.

2.4. Aging Protocol

We applied an aging protocol in two steps. In the first step, all three cells were cycled four times in order to estimate their initial capacity. These data were necessary for the SoH analysis, described in the next section. The potentiostatic electrochemical impedance

spectroscopy (PEIS) technique was applied, using the Modulo Bat (MB) technique to improve the analysis of our LIB systems, particularly during dynamic testing scenarios such as the charge and discharge cycles. The MB technique incorporates features that allow impedance measurements during ongoing charge or discharge, which are traditionally difficult due to the presence of a DC current. At the same time, it synchronizes impedance measurements with the varying states of charge or discharge, ensures regular intervals of impedance data collection without disrupting the natural cycling process, and allows a small AC signal to be superimposed on the DC voltage or current during cycling, thus capturing the impedance at specific moments and providing insights into its dynamic behaviors. The combination of these techniques reflect the gradual degradation of the LIBs' performance over time and cycles.

In our PEIS sequence under MB, the sinus signal was imposed only around the DC potential near to the equilibrium state, taking into account that this mechanism can easily lead to overcharging in a fully charged Li-ion cell, particularly at low frequencies (below 50 mHz). As such, the PEIS settings in the stand-alone module gave us permission to superimpose a sinus signal over a fixed DC potential, E, that was sufficiently small, so the upper voltage limit was not surpassed at low frequencies. A potential of 10 mV was imposed within a frequency length of 10 kHz–5 mHz, while the sinus amplitude was set to 20 mV. We also applied 30 min of relaxation before each PEIS measurement to the aging protocol.

By monitoring the voltage change difference after 30 min, we obtained a value smaller than 0.1%, indicating that the cells are in a stable state. The initial capacity of all three LIBs had closely related values, namely, 3.27 for B1, 3.26 for B2, and 3.24 for B3. The workflow diagram presented below in Figure 3 shows schematically the aging procedure applied in this investigation.

Figure 3. Steps initiated for battery aging.

3. Results

3.1. SoH Dependence in Fast Charging and Fast Discharging Operations

The SoH cycling evolution in the B1, B2, and B3 batteries was analyzed according to their distinct fast charging and fast discharging rates. The goal was to gain insights into their overall condition and remaining capacity relative to their initial states. It is well known that, over time, lithium-ion cells degrade due to various chemical and physical processes, leading to a reduction in their performance. Thus, we aimed to understand the SoH behavior under particular conditions in order to further predict the battery lifetime, optimize battery usage, and improve safety conditions. This offers predictive maintenance to avoid unexpected failures and also an indication of battery replacement necessity.

The following formula was employed for the SoH measurement, as already performed elsewhere [65,66]:

$$\mathrm{SoH} = \frac{C_{\mathrm{discharged}}}{C_{\mathrm{initial}}} \times 100\ [\%] \quad (2)$$

The capacity testing through the controlled (fast) charge–discharge rates of B1, B2, and B3 is shown in terms of the SoH vs. the cycle number in Figure 4a. Here, we define the charge or discharge current as a function of the capacity. As can be seen, when the I_{charge} is increased from 1C to 1.5C and 2C, the SoH decay curves behave differently, even if $I_{discharge}$ remains constant at 2C. For B1, a smooth decay curve was obtained, and around 200 cycles were required until the battery was exhausted. An approximate half-cycle number of around 95 was obtained for the B2 cell when the I_{charge} was increased to a fast 1.5C, thus reducing the battery exhausting period by more than half. It seems that the gradual loss of the B2 charge storage capacity led to a significant reduction in performance, significantly affecting the loss of active lithium ions (i.e., lithium becomes trapped in the electrode side reactions), electrode degradation through structural damage to cathode or anode materials, or SEI (solid electrolyte interface) layer growth on the anode. Degradation due to repeated charge–discharge cycles occurred extremely fast for B3 when the fast charge rate of 2C was equal to the deep discharge rate. The SoH curve of B3 with error bars is shown in Figure 4b. The internal operation of inserting lithium ions, embedded in the negative electrode during charging, into the positive electrode during discharge became extremely difficult.

As a direct consequence, the B3 cell damage occurred very fast, after ~25 cycling steps; thus, we assumed that the cell reversal had caused an electrical short. Within this fast-cycling process, the stress suffered is near to the maximum permissible tolerance, leading to the fast degradation of the electrode's elasticity. These results demonstrate that by increasing the I_{charge} from 1C to 1.5C (with a 2C discharge rate), the battery lifetime is reduced by ~50%, while in the case of fast charge/discharge rates of 2C, the lifetime performance decreases by almost ~70%. As such, the capacity loss accelerates quickly when the charge rates increase from 1C to 1.5C and 2C, offering concrete data on the lifetime performance and efficiency of our LIBs in fast charging–fast discharging cycling operations.

It should be mentioned that all the measurements were performed until the batteries were completely discharged; thus, we aimed to gain insights into how much of the battery's lifetime available energy had been consumed and how much was left, anticipating further performance or replacement of the battery. A clear indication of battery degradation based on cycling rates can be easily seen on Figure 4, starting directly from the beginning, at 100% SoH, when a steeper increase for B1, B2, and B3 was obtained. Moreover, for the B3 cell, the last discharge rate can only go up to ~80% SoH, as the battery charge rate can no longer support faster degradation.

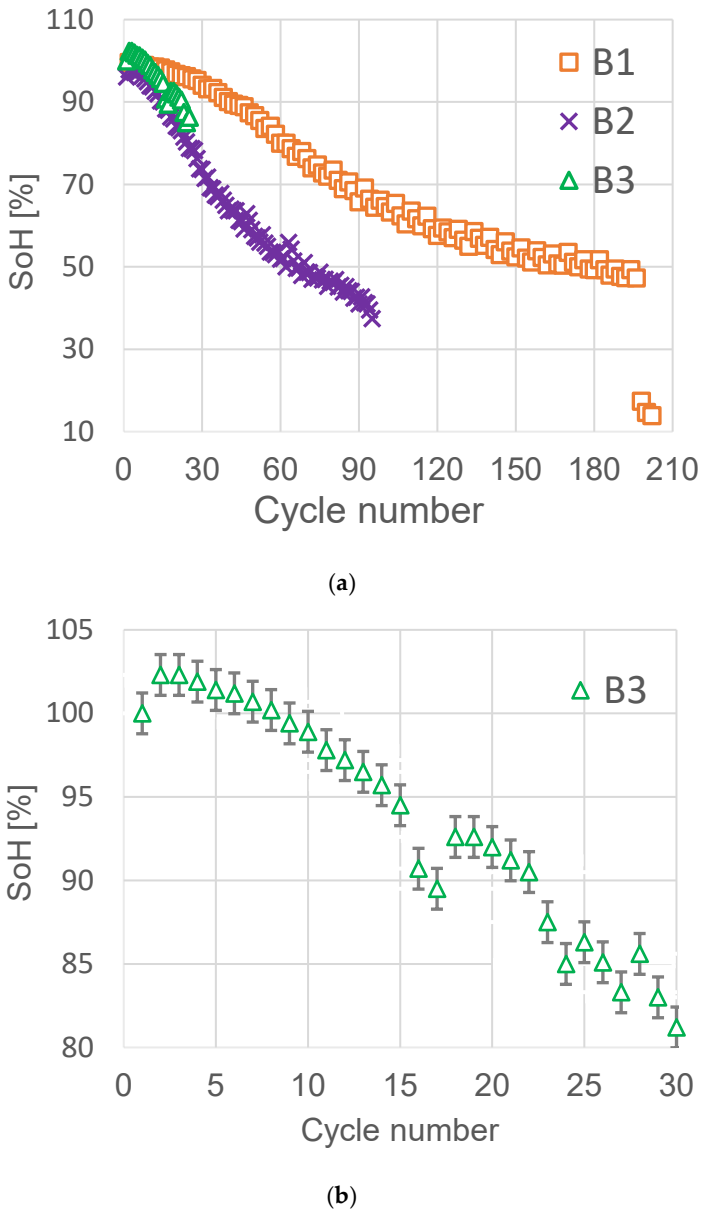

Figure 4. (**a**) The SoH vs. the cycle number in the B1, B2, and B3 batteries; (**b**) error bars for B3.

In the second step, in order to evaluate and compare the stability of the B1, B2, and B3 cells, we performed an analysis of the coulombic efficiency (CE) [67]. This parameter can be defined as the ratio of the charge delivered during the discharge, $Q_{discharge}$, to that stored during the charge, Q_{charge}:

$$CE = \frac{Q_{dis}}{Q_{cha}} \times 100\ [\%] \quad (3)$$

while the accuracy of the CE determination can be affected by the precision in the Q measurement. The charge delivered or stored during the discharge/charge at a constant current is thus defined by the following [68]:

$$Q_{dis/cha} = I \times \Delta t^4 [Ah] \quad (4)$$

where I represents the discharge/charge current, and Δt is the time interval during discharge/charge.

Therefore, we used the CE in order to quantify the capacity of the batteries to restitute during discharge the energy stored during the charge. However, the CE can only be computed when the charge occurs first and then the discharge. In Figure 5, we illustrate the coulombic efficiency of our cells through the curve shape of the B1 cell, which can be directly correlated with B1 in Figure 4.

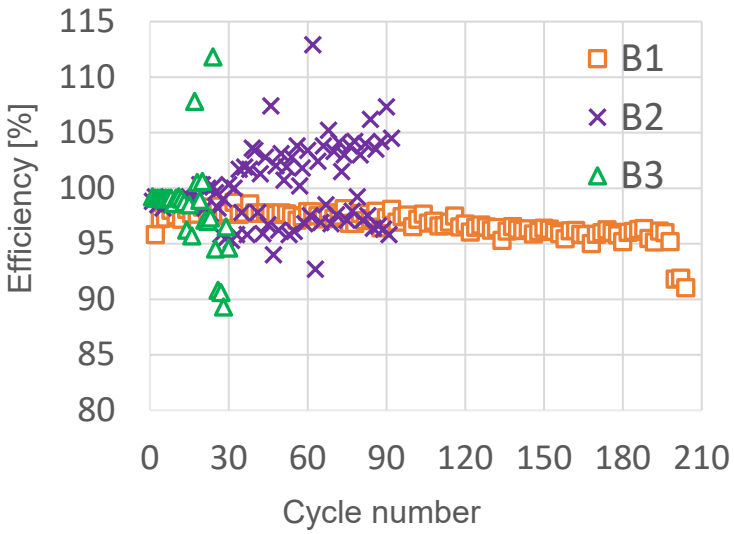

Figure 5. The coulombic efficiency of the LIB cells.

A similar smooth decrease in efficiency is observed for B1 in the longest lasting cycling, while for B2 and B3, a much more dispersed behavior can be noticed. Again, this is in agreement with the SoH analysis, in which the smoothness of B2 and B3 is not as pronounced as for B1. By increasing the charge rate and using the already fast discharge rate, the LIB efficiency vs. cycle number, as plotted in Figure 5, highlights how the energy storage capability of B1, B2, and B3 decays, even after a few cycling steps. If we obtain a coulombic efficiency of ~97% for B1, the range increase for B2 is between 93% and 113%, while for B3, the radius increases by between 88% to 112%.

To further correlate the behavior of the Li-ion batteries under fast-charging and fast-discharging conditions, impedance traces were calculated, as shown in Figure 6. We can see that impedance is charging-rate dependent. As the charging rate goes up, the impedance curve of the battery gradually increases, although the minimum impedance value always falls at around 3000 Hz, unconstrained by the charge or discharge rate. Each charge rate determines an increase of one order of magnitude in the cell impedance. A charging rate of 2C determines an obvious impedance growth rate of up to 23%.

3.2. $Q–Q_0$ Total Charge Analysis

We performed a total charge analysis, in which the $Q–Q_0$ parameter can be regarded as the total charge exchanged since the beginning of the experiment, representing the ratio between the energy stored and the energy dissipated per cycle, or as a product of the electric current flowing throughout the battery and the time duration. Our goal was to identify a reliable method able to predict the aging status of lithium-ion cells based on the charge/discharge rates, thus greatly decreasing the number of elements to be studied (for example, Nyquist plots within their Randle equivalent circuit elements). In order to compare and/or correlate the cells' tendencies as an indication of the behavior of the cell under cycling conditions, we used the data results after finishing the aging procedure. As a setup protocol, a small sinusoidal signal was applied around a DC potential in the frequency range of 0.2–200 Hz, while the amplitude of the voltage signal was set to 3 mV.

Thus, we have taken into account that the magnitude of the net charge on the plate will increase with time, following the equation below [69]:

$$Q = Q_0 \cdot \left(1 - e^{\frac{t}{\tau}}\right) \text{ [Ah]} \quad (5)$$

in which τ is considered the time constant of the circuit.

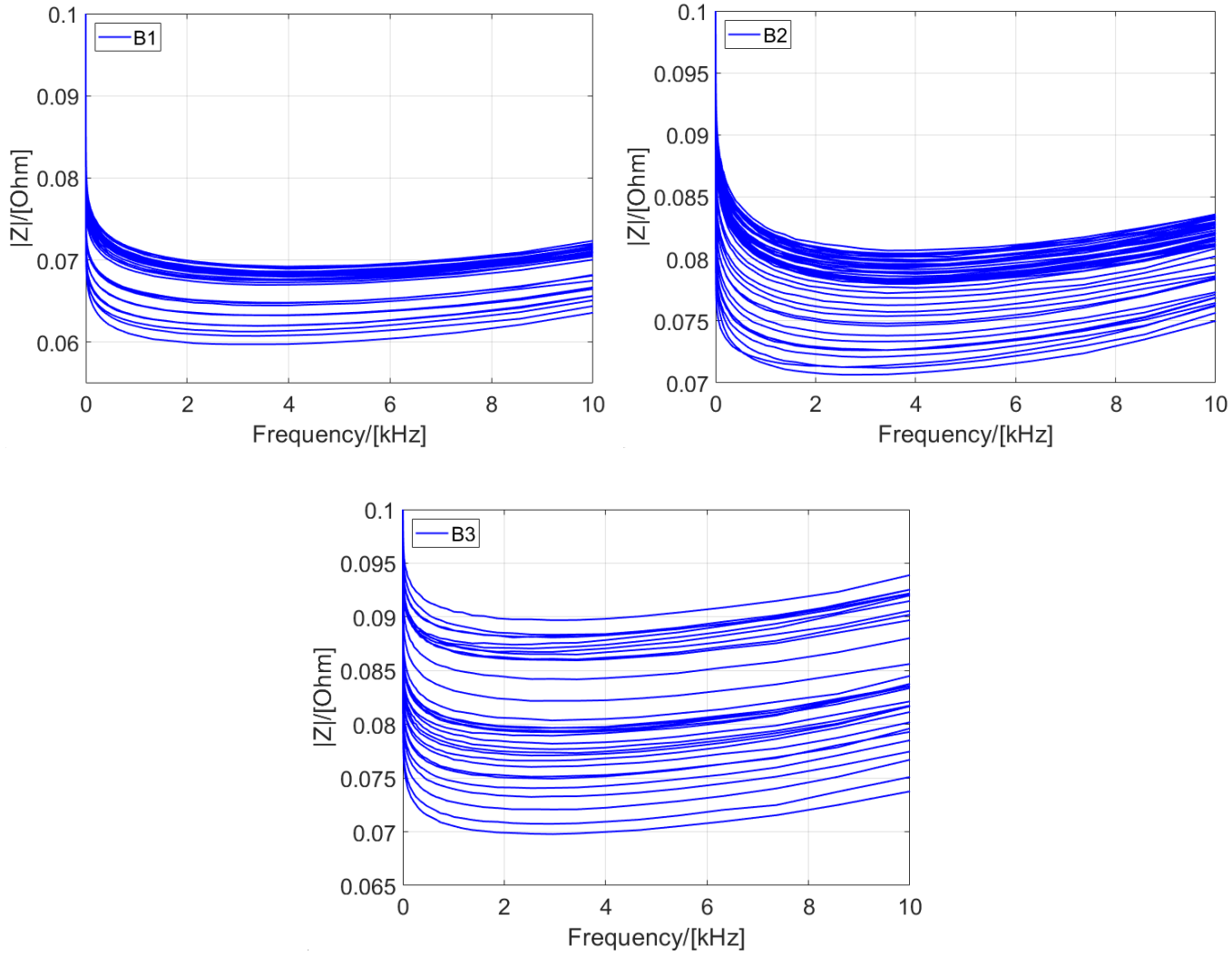

Figure 6. Impedance versus frequency.

By applying fast charge/discharge rates to B1, B2, and B3, we tried to gain insights into the batteries' lifespan, in which performance may be significantly affected and safety risks might arise from charging or discharging above the specified voltage. In Figure 7, we show the total charge results for our cells.

If we look at Figure 7—top, we can observe a smooth curve for the B1 cell type similar to that in the previous section (see Figures 4 and 5), regardless of whether we look at the Q_{charge} or $Q_{discharge}$. This means that at a lower I_{charge}, the process of lithium-ion extraction from one electrode and the intercalation to the other is not affected during the aging procedure, thus emphasizing a smooth trend.

This is not the case for the B2 or, in particular, the B3 cells (see Figure 7—middle and bottom), in which the fast-cycling rates emphasize more dispersive curves. It is clear that the process of inserting the lithium ions, embedded in the negative electrode during charging, into the positive electrode during the discharge, is significantly affected. Specifically, in

Figure 7, the LIBs with the longer cycle life have a reduced charge/discharge growth during the PEIS cycling measurements (Figure 7—top). When the fluctuations in Q_{charge} and $Q_{discharge}$ become more and more pronounced (Figure 7—middle and bottom), the total charge balance clearly affects the LIB efficiency, which is in full agreement with the results described in Section 3.1. Because the LIBs have a high voltage per cell, with tighter voltage tolerances and the absence of a trickle or float charge at full charge, they cannot easily accept the overcharge. By increasing the charge rate from B1 to B2 and B3 and fully charging the cells, an additional high voltage is added that stresses the battery more and more. This can be translated into a shorter lifetime, as was shown already here. In any case, choosing a lower voltage threshold, or eliminating the saturation charge altogether, will clearly prolong the battery aging process.

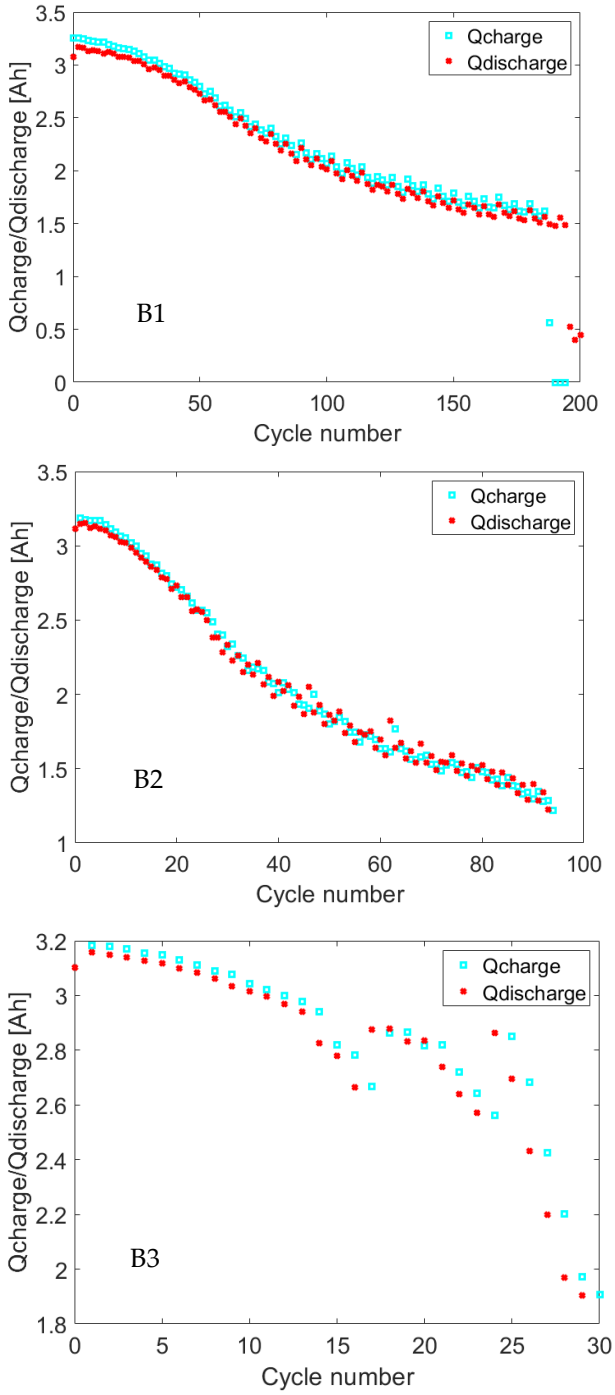

Figure 7. Total charge behavior during the first PEIS analysis: B1 (**top**), B2 (**middle**), and B3 (**bottom**).

3.3. Energy Consumption in the Charged and Discharged State

Energy consumption in the charged and discharged state gives a good indication of the battery lifecycle, being fundamentally related to how the battery stores and releases electrical energy. In particular, in the charged state (we employed three different charge rates), the LIB has electrical energy stored in the form of chemical potential energy. When our cells are charged, lithium ions move from the positive electrode (cathode) to the negative electrode (anode) through the electrolyte. This process is accompanied by the flow of electrons through an external circuit, which allows energy to be supplied to devices like smartphones, electric vehicles, and other portable devices, as we mentioned in Section 3.1. The energy consumed during charging can be expressed as follows [70]:

$$E = V \cdot I \cdot t \ [Wh] \quad (6)$$

where E represents the energy in watt-hours (Wh), V is the voltage, I is the current, and t is the charging time. It should be mentioned that the efficiency of charging is not 100%, and losses occur in the form of heat due to internal resistance, meaning that the total energy consumed from the power source will be higher than the energy stored in the battery. Regarding the discharge state, the battery supplies energy by allowing lithium ions to move from the anode back to the cathode. This flow of ions drives the movement of electrons through the external circuit, which powers the connected devices. The discharge process converts chemical energy back into electrical energy, where the energy E is released by the LIB and consumed by the device. Also in this case, we have energy loss due to internal resistance, and the efficiency of energy release is not perfect. This loss results in heat generation, reducing the effective energy output. As such, in both processes, inefficiencies appear due to internal resistance and other factors, but the overall energy consumption will be higher than the energy that is effectively stored or used due to these losses.

In Figure 8, the resultant values (left) are shown together with the dE—the difference between the charge and the discharge states (right). The shifting of the curves that appears now in Figure 8 for B1, B2, and B3 (a), in comparison with those illustrated in Figure 7, comes from the V factor, but the trend is very similar. It is known that LIBs operate within a specific voltage range (typically from around 4.2 V when fully charged to around 3.0 V when discharged). As the voltage decreases during discharge, the amount of energy available from the battery decreases, even if the current is constant.

Moreover, the continuous high discharge rates rapidly deplete the battery capacity, reducing the energy storage capability and long-term performance. The battery efficiency decreases dramatically when losses appear because the internal resistance causes more and more heat to be produced during both fast charging and discharging. The difference, dE, between the energy in charged mode versus discharged mode has been captured in Figure 8b—B1, B2, and B3. For the 1C charge rate, the dE is quasi-constant around the value of 3 Wh throughout the interval, whereas for the 1.5C and 2C charging values, the dE increases above 3.5 Wh and has a descending irregular trend. By fast discharging, up to 30% of the energy is lost, as seen in Figure 8b—B3. In other words, discharging the battery too much (deep discharge) will clearly result in a reduced voltage, lowering the amount of usable energy.

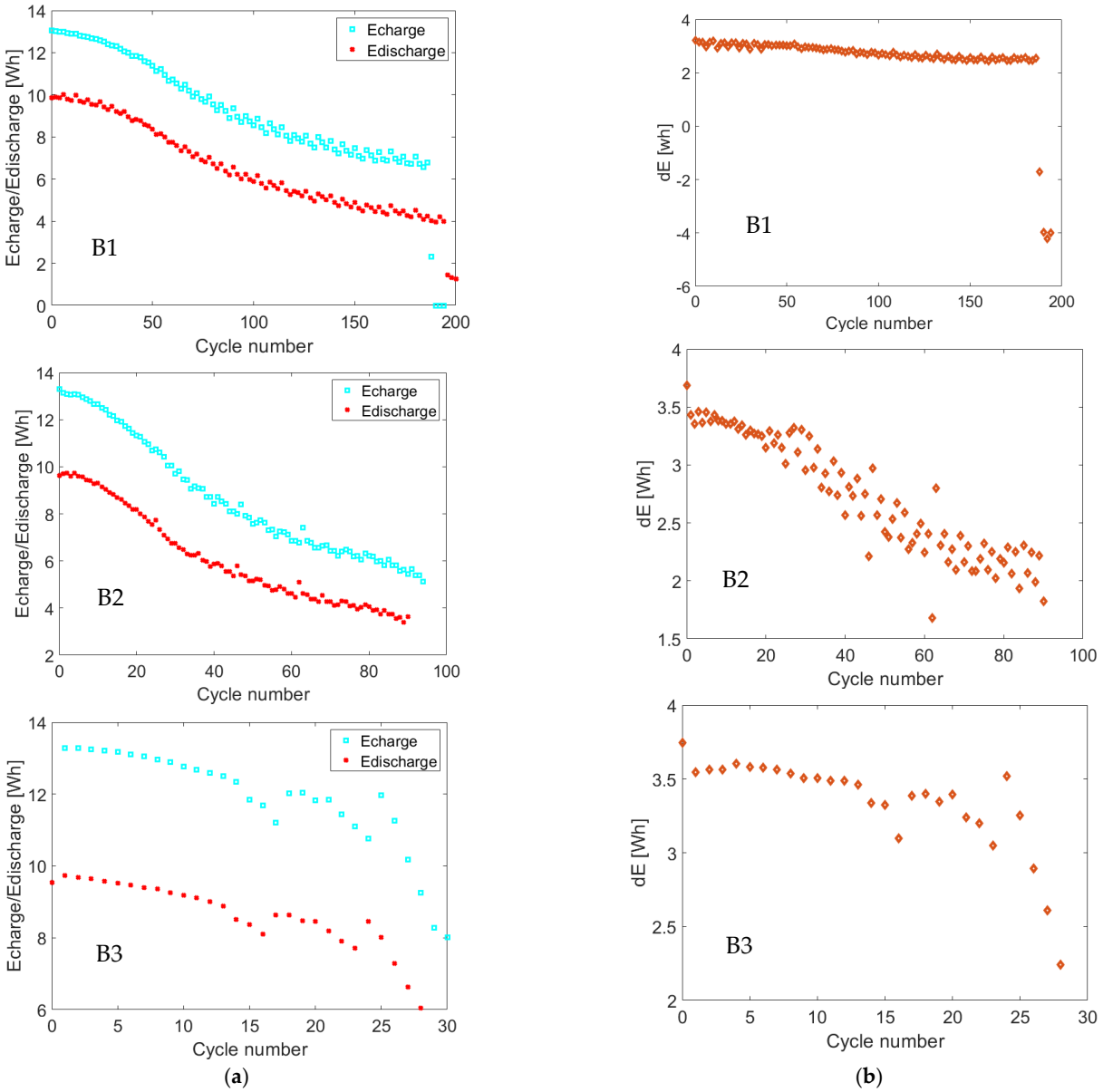

Figure 8. (**a**) Energy consumption in the charged and discharged state of B1, B2, and B3; (**b**) dE—difference between the charge and the discharge states of B1, B2, and B3.

3.4. Spline Interpolation

Spline interpolation is a good choice for non-linear data point interpolation. Smoothing spline interpolation uses a special type of polynomial called a spline. The smoothing spline *fs* minimizes the following expression [71]:

$$fs = p_s \cdot \sum_{i=1}^{n} |y_i - f(x_i)|^2 + \left(1 - p_s \int \left|\frac{d^2 f}{dt^2}\right|^2 dt\right) \quad (7)$$

where p_s is the smoothing parameter, n is the number of x entries, and y is the vector of data values. The weights were considered to be 1. The sum of the first member measures the error, and the integral determines the roughness of the function. In order to evaluate the goodness of fit, one indicator has been determined, and that is the root mean squared error (RMSE). The RMSE indicator evaluates the capability of the model to predict the target

value. Basically, it measures the difference between the values predicted by the model and the real values [72]:

$$\mathrm{RMSE} = \sqrt{\frac{\sum_{i=1}^{n}(y_i - f(x_i))^2}{n}} \quad (8)$$

The rate of change of energy decay in each case was monitored by determining the slope in both the charged and discharged mode. A negative slope defines the decrease in energy as the number of cycles increases. As such, in Table 2, the calculated spline RMSE fit parameters for B1, B2, and B3 are shown.

In Figure 9, the spline interpolation data for both E_{charge} and $E_{discharge}$ are shown, emphasizing the resultant values of the B1, B2, and B3 curves.

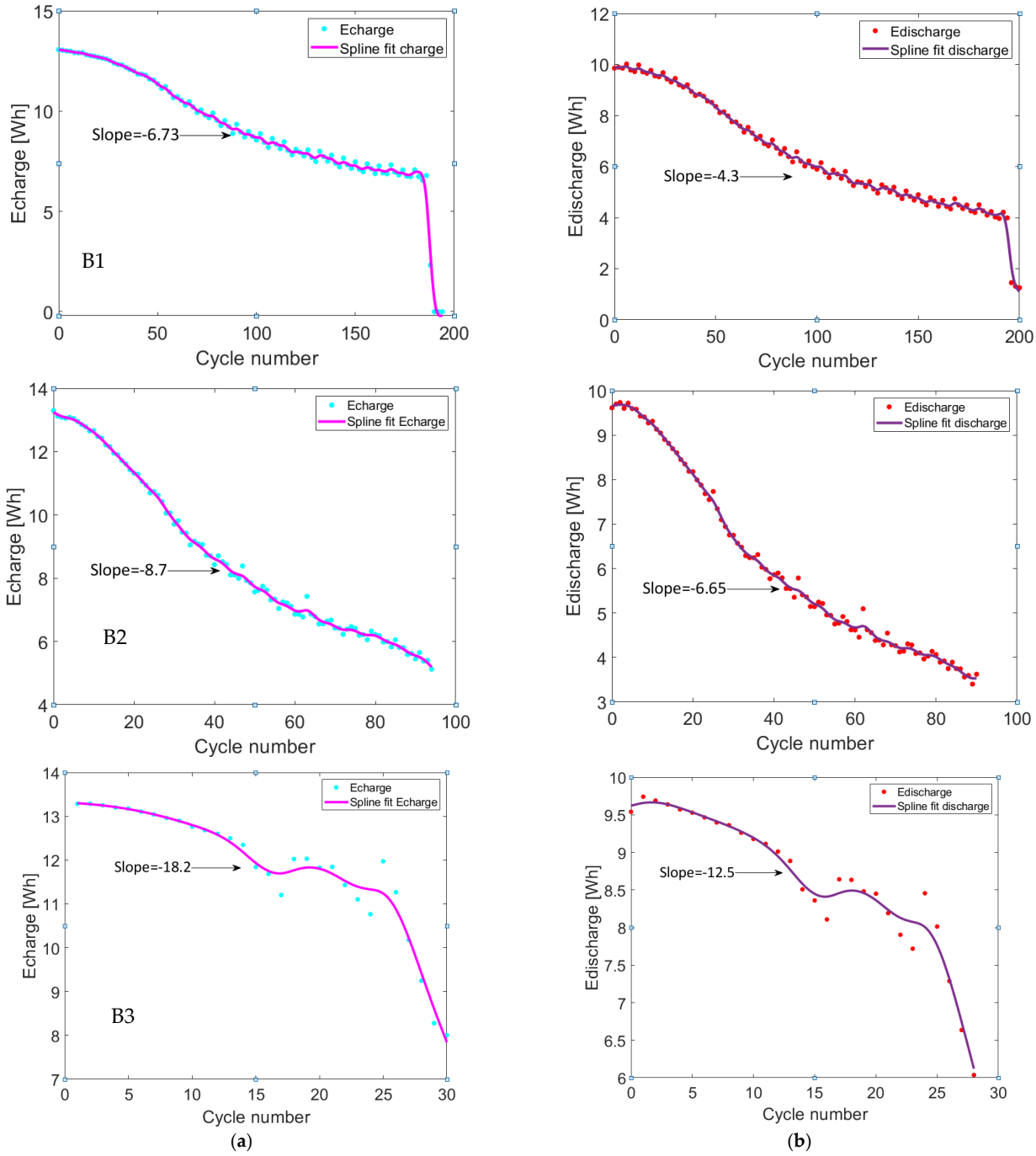

Figure 9. Spline interpolation of the B1, B2, and B3 energy curves: (**a**) in charge mode; (**b**) in discharge mode.

Table 2. Spline RMSE fit parameters.

RMSE	B1	B2	B3
Charged	0.242	0.288	0.121
Discharged	0.180	0.184	0.107

The smoothing parameter, p_s, was set to 0.312 to achieve the fidelity of the data and the smoothness of the curve. It can be noticed that the model fit data accurately. The RMSE values stayed below 0.3, a slightly better fit being obtained for the discharged modes. As the current rate increases the slope decreases. The slope is smaller in the charged mode for all cases, as it starts from the maximum energy and decreases toward zero at the end of cycling. In B3, the slope decreased by 37% compared with the slope determined for B1.

In Table 3, we present the battery performance indicators in order to provide a clear understanding of their relative performances.

Table 3. LIB performance indicators.

Battery	B1	B2	B3
Life cycles	200	95	30
SOH [%]	14	37.4	81.6
Min. impedance [%]	0.07	0.08	0.09
Rate of energy decrease charge/discharge	−6.73/−4.3	−8.7/−6.65	−18.2/−12.5

4. Conclusions

By employing EIS methodology, the cycle life performance and the influence of the C-rate on the charge/discharge processes were investigated when I_{charge} evolved from 1C, to 1.5C and 2C and $I_{discharge}$ was set to 2C in all cases. First, we aimed to assess and monitor the batteries' SoH at fast charge/discharge rates, as this parameter is a highly demanded attribute for advanced battery management systems (BMS). Capacity testing of the B1, B2, and B3 batteries, shown in terms of the SoH vs. the cycle number, was performed, emphasizing a different decay curve behavior, from a smooth fall in the case of the B1 cell type to a more disorderly disposition for B2, and even more so for the B3 type. Within the I_{charge} increment, we clearly observed a decrease in their lifetime performance and a fast-aging process; for B1, around 200 cycles were required until the battery was exhausted, while for B2, approximately half the number of cycles (around 90) were necessary, thus reducing the battery exhausting period by more than half. When fast charging/fast discharging 2C was applied, the B3 cell degradation occurred very rapidly, after ~30 cycling steps, assuming that the suffered stress was near to the maximum permissible tolerance, leading to fast degradation. As a consequence, when increasing the I_{charge} from 1C to 1.5C, both with a 2C discharge rate, the battery lifetime was reduced by ~50%, while in the case of fast charge/discharge rates of 2C, the lifetime performance decreased by almost ~80%. These results show how fast capacity loss accelerates when the charge rates increase, offering concrete data on the lifespan of our LIBs. The SoH determination, as a critical parameter of stability, provides a pre-warning of a failing LIB, enabling maintenance/replacement before damage actually occurs.

Continuing with the SoH interpretation, we monitored the coulombic efficiency (CE) in order to express the capacity of the batteries to restitute during discharge the energy stored during the charge. This is in full agreement with the LIBs' efficiency vs. cycle number behavior we observed, highlighting the different decay rates of the energy storage capability

in B1, B2, and B3. A coulombic efficiency of ~97% was obtained for B1, while for B2 and B3, the range increased by between 93% and 113% and 88% to 112%, respectively. It seems that as the battery impedance reaches a certain level, the capacity significantly decreases until it cannot provide the required charge. Impedance traces were also employed, showing their dependency in terms of charging rates. To this end, for the three charge rates considered, the end of battery life was quantified as an impedance of 0.07, 0.08, and 0.09 Ohm and an SoH of 14%, 37.4%, and 80%, respectively.

Second, we performed a total charge Q–Q_0 analysis. A good agreement with the SoH data was achieved, in which a similar smooth curve for B1 was obtained and more dispersive fluctuations for B2 and B3 cells were seen. During the PEIS cycling measurements, a reduced charge/discharge growth was related to a longer cycle life, while the fluctuations in the total charge balance clearly affected the B2 and B3 efficiency. By increasing the charge rates and charging the cells at 100% SoC, an additional high voltage was added that affected the cells more and more. As a direct conclusion of this result, choosing a lower voltage threshold, or eliminating the saturation charge altogether, will definitely extend the LIBs' aging process.

Finally, energy consumption estimation was performed to gain insights into how the batteries store and release electrical energy depending on their charge/discharge rates. Through I_{charge} increments, the LIBs' efficiency decreased dramatically when losses appeared because the internal resistance caused more and more heat to be produced during both fast charging and discharging. By performing a dE analysis, which represents the difference between the energy in charged and discharged mode, we observed that for B1, this element is quasi-constant around the value of 3 Wh throughout the interval, whereas for the B2 and B3 cells, the dE increased above 3.5 Wh and had a descending irregular trend. Moreover, by fast discharging, up to 30% of the energy was lost, indicating that discharging the battery too much will clearly result in a reduced voltage, which decreases the amount of usable energy. The continuous fast discharge applied to our LIBs rapidly depleted cell capacity, thus reducing their energy storage capability and long-term performance. The rate of energy decay is directly proportional to the charge rates, and the spline interpolation was verified through RMSE fit parameters.

Author Contributions: O.B.: methodology, validation, formal analysis, investigation, resources, data curation, and writing—original draft preparation. A.C.: conceptualization, investigation, writing—original draft preparation, writing—review and editing, visualization, supervision, project administration, and funding acquisition. All authors have read and agreed to the published version of the manuscript.

Funding: This study was financially supported by the MCID Core Program within the National Plan for Research Development and Innovation 2022–2027 project PN 23 24 01 04.

Data Availability Statement: Data are contained within the article.

Conflicts of Interest: The authors declare no conflicts of interest.

References

1. Manthiram, A. A reflection on lithium-ion battery cathode chemistry. *Nat. Commun.* **2020**, *11*, 1550. [CrossRef] [PubMed]
2. Stallard, J.C.; Wheatcroft, L.; Booth, S.G.; Boston, R.; Corr, S.A.; De Volder, M.F.; Inkson, B.J.; Fleck, N.A. Mechanical properties of cathode materials for lithium-ion batteries. *Joule* **2022**, *6*, 984–1007. [CrossRef]
3. Bridgewater, G.; Capener, M.J.; Brandon, J.; Lain, M.J.; Copley, M.; Kendrick, E. A comparison of Lithium-Ion cell performance across three different cell formats. *Batteries* **2021**, *7*, 38. [CrossRef]
4. Zhao, S.; Guo, Z.; Yan, K.; Wan, S.; He, F.; Sun, B.; Wang, G. Towards high-energy-density lithium-ion batteries: Strategies for developing high-capacity lithium-rich cathode materials. *Energy Storage Mater.* **2021**, *34*, 716–734. [CrossRef]

5. Zhang, X.; Han, Y.; Zhang, W. A Review of Factors Affecting the Lifespan of Lithium-ion Battery and its Health Estimation Methods. *Trans. Electr. Electron. Mater.* **2021**, *22*, 567–574. [CrossRef]
6. Peng, X.; Lin, Y.; Wang, Y.; Li, Y.; Zhao, T. A lightweight localized high-concentration ether electrolyte for high-voltage Li-Ion and Li-metal batteries. *Nano Energy* **2022**, *96*, 107102. [CrossRef]
7. Liu, G.; Wan, W.; Nie, Q.; Zhang, C.; Chen, X.; Lin, W.; Wei, X.; Huang, Y.; Li, J.; Wang, C. Controllable long-term lithium replenishment for enhancing energy density and cycle life of lithium-ion batteries. *Energy Environ. Sci.* **2024**, *17*, 1163–1174. [CrossRef]
8. Xiao, S.; Huang, L.; Lv, W.; He, Y.-B. A highly efficient ion and electron conductive interlayer to achieve low self-discharge of lithium-sulfur batteries. *ACS Appl. Mater. Interfaces* **2022**, *14*, 1783–1790. [CrossRef]
9. He, J.; Meng, J.; Huang, Y. Challenges and recent progress in fast-charging lithium-ion battery materials. *J. Power Sources* **2023**, *570*, 232965. [CrossRef]
10. Rodrigues, M.-T.F.; Babu, G.; Gullapalli, H.; Kalaga, K.; Sayed, F.N.; Kato, K.; Joyner, J.; Ajayan, P.M. A materials perspective on Li-ion batteries at extreme temperatures. *Nat. Energy* **2017**, *2*, 17108. [CrossRef]
11. Yudhistira, R.; Khatiwada, D.; Sanchez, F. A comparative life cycle assessment of lithium-ion and lead-acid batteries for grid energy storage. *J. Clean. Prod.* **2022**, *358*, 131999. [CrossRef]
12. Ayeng'O, S.P.; Schirmer, T.; Kairies, K.-P.; Axelsen, H.; Sauer, D.U. Comparison of off-grid power supply systems using lead-acid and lithium-ion batteries. *Sol. Energy* **2018**, *162*, 140–152. [CrossRef]
13. Hu, J.; Zhang, C.; Wang, Y.; Zhang, P.; Zhang, L.; Wang, J.; Lao, L. Multisource information fusion based parameterization study of lithium-ion battery electrolyte leakage. *J. Energy Storage* **2023**, *73*, 109017. [CrossRef]
14. Tran, M.-K.; DaCosta, A.; Mevawalla, A.; Panchal, S.; Fowler, M. Comparative study of equivalent circuit model performance in four common lithium-ion batteries: LFP, NMC, LMO, NCA. *Batteries* **2021**, *7*, 51. [CrossRef]
15. Wu, Q.; Zhang, B.; Lu, Y. Progress and perspective of high-voltage lithium cobalt oxide in lithium-ion batteries. *J. Energy Chem.* **2022**, *74*, 283–308. [CrossRef]
16. Baazizi, M.; Karbak, M.; Aqil, M.; Sayah, S.; Dahbi, M.; Ghamouss, F. High-valence surface modified LMO cathode materials for lithium-ion batteries: Diffusion kinetics and operando thermal stability investigation. *ACS Appl. Mater. Interfaces* **2023**, *15*, 40385–40396. [CrossRef]
17. Li, T.; Yuan, X.-Z.; Zhang, L.; Song, D.; Shi, K.; Bock, C. Degradation mechanisms and mitigation strategies of nickel-rich NMC-based lithium-ion batteries. *Electrochem. Energy Rev.* **2020**, *3*, 43–80. [CrossRef]
18. Zeng, C.; Zheng, R.; Fan, F.; Wang, X.; Tian, G.; Liu, S.; Liu, P.; Wang, C.; Wang, S.; Shu, C. Phase compatible surface engineering to boost the cycling stability of single-crystalline Ni-rich cathode for high energy density lithium-ion batteries. *Energy Storage Mater.* **2024**, *72*, 103788. [CrossRef]
19. Zeng, C.; Fan, F.; Zheng, R.; Wang, X.; Tian, G.; Liu, S.; Liu, P.; Wang, C.; Wang, S.; Shu, C. Structure and Charge Regulation Strategy Enabling Superior Cycling Stability of Ni-Rich Cathode Materials. *ACS Appl. Mater. Interfaces* **2024**, *16*, 11377–11388. [CrossRef]
20. Fan, F.; Zheng, R.; Zeng, T.; Xu, H.; Wen, X.; Wang, X.; Tian, G.; Wang, S.; Zeng, C.; Xiang, W.; et al. Cation-ordered Ni-rich positive electrode material with superior chemical and structural stability enabled by atomic substitution for lithium-ion batteries. *Chem. Eng. J.* **2023**, *477*, 147181. [CrossRef]
21. Yan, Y.; Shu, C.; Zheng, R.; Li, M.; Ran, Z.; He, M.; Hu, A.; Zeng, T.; Xu, H.; Zeng, Y. Modulating Sand's time by ion-transport-enhancement toward dendrite-free lithium metal anode. *Nano Res.* **2022**, *15*, 3150–3160. [CrossRef]
22. Li, W.; Wang, H.; Zhang, Y.; Ouyang, M. Flammability characteristics of the battery vent gas: A case of NCA and LFP lithium-ion batteries during external heating abuse. *J. Energy Storage* **2019**, *24*, 100775. [CrossRef]
23. Julien, C.M.; Mauger, A. Fabrication of Li4Ti5O12 (LTO) as Anode Material for Li-Ion Batteries. *Micromachines* **2024**, *15*, 310. [CrossRef]
24. Liu, J.; Zhou, Y.; Yan, T.; Gao, X.-P. Perspectives of high-performance Li-S battery electrolytes. *Adv. Funct. Mater.* **2024**, *34*, 2309625. [CrossRef]
25. Xia, F.; Wang, K.; Chen, J. State of health and remaining useful life prediction of lithium-ion batteries based on a disturbance-free incremental capacity and differential voltage analysis method. *J. Energy Storage* **2023**, *64*, 107161. [CrossRef]
26. Lin, Q.; Wang, J.; Xiong, R.; Shen, W.; He, H. Towards a smarter battery management system: A critical review on optimal charging methods of lithium ion batteries. *Energy* **2019**, *183*, 220–234. [CrossRef]
27. Li, Y.; Guo, H.; Qi, F.; Guo, Z.; Li, M. Comparative Study of the Influence of Open Circuit Voltage Tests on State of Charge Online Estimation for Lithium-Ion Batteries. *IEEE Access* **2020**, *8*, 17535–17547. [CrossRef]
28. Zhu, J.; Wang, Y.; Huang, Y.; Gopaluni, R.B.; Cao, Y.; Heere, M.; Muhlbauer, M.J.; Mereacre, L.; Dai, H.; Liu, X.; et al. Data-driven capacity estimation of commercial lithium-ion batteries from voltage relaxation. *Nat. Commun.* **2022**, *13*, 2261. [CrossRef]
29. Choi, W.; Shin, H.-C.; Kim, J.M.; Choi, J.-Y.; Yoon, W.-S. Modeling and Applications of Electrochemical Impedance Spectroscopy (EIS) for Lithium-ion Batteries. *J. Electrochem. Sci. Technol.* **2020**, *11*, 1–13. [CrossRef]

30. Takeno, M.; Fukutsuka, T.; Miyazaki, K.; Abe, T. Investigation of electronic resistance in lithium-ion batteries by AC impedance spectroscopy. *J. Electrochem. Soc.* **2017**, *164*, A3862–A3867. [CrossRef]
31. Huang, H.; Meng, J.; Wang, Y.; Feng, F.; Cai, L.; Peng, J.; Liu, T. A comprehensively optimized lithium-ion battery state-of-health estimator based on Local Coulomb Counting Curve. *Appl. Energy* **2022**, *322*, 119469. [CrossRef]
32. Mayilvahanan, K.S.; Takeuchi, K.J.; Takeuchi, E.S.; Marschilok, A.C.; West, A.C. Supervised learning of synthetic Big Data for Li-ion battery degradation diagnosis. *Batter. Supercaps* **2022**, *5*, e202100166. [CrossRef]
33. Zhang, Y.; Li, Y.-F. Prognostics and health management of Lithium-ion battery using deep learning methods: A review. *Renew. Sustain. Energy Rev.* **2022**, *161*, 112282. [CrossRef]
34. Hossain, M.; Haque, M.; Arif, M. Kalman filtering techniques for the online model parameters and state of charge estimation of the Li-ion batteries: A comparative analysis. *J. Energy Storage* **2022**, *51*, 104174. [CrossRef]
35. Motapon, S.N.; Lachance, E.; Dessaint, L.-A.; Al-Haddad, K. A Generic Cycle Life Model for Lithium-Ion Batteries Based on Fatigue Theory and Equivalent Cycle Counting. *IEEE Open J. Ind. Electron. Soc.* **2020**, *1*, 207–217. [CrossRef]
36. Carnovale, A.; Li, X. A modeling and experimental study of capacity fade for lithium-ion batteries. *Energy AI* **2020**, *2*, 100032. [CrossRef]
37. Vedel, P.; Hubka, L. Linear regression model of Li-ion battery capacity losing rate based on equivalent circuit model parameters and operation modes. In Proceedings of the 2022 International Conference on Smart Systems and Technologies (SST), Osijek, Croatia, 19–21 October 2022; pp. 243–248.
38. Wang, G.; Lyu, Z.; Li, X. An optimized random forest regression model for Li-ion battery progonostics and health management. *Batteries* **2023**, *9*, 332. [CrossRef]
39. Yao, P.; Liu, X. Electrochemical and thermal analysis of lithium-ion batteries based on variable solid-state diffusion coefficient concept. *World Electr. Veh. J.* **2024**, *15*, 416. [CrossRef]
40. Dong, Y.; Chen, K.; Zhang, G.; Li, R. Joint estimation of state of charge and state of health of lithium-ion batteries based on stacking machine learning algorithm. *World Electr. Veh. J.* **2024**, *15*, 75. [CrossRef]
41. Tran, M.-K.; Mathew, M.; Janhunen, S.; Panchal, S.; Raahemifar, K.; Fraser, R.; Fowler, M. A comprehensive equivalent circuit model for lithium-ion batteries, incorporating the effects of state of health, state of charge, and temperature on model parameters. *J. Energy Storage* **2021**, *43*, 103252. [CrossRef]
42. Ding, X.; Zhang, D.; Cheng, J.; Wang, B.; Luk, P.C.K. An improved Thevenin model of lithium-ion battery with high accuracy for electric vehicles. *Appl. Energy* **2019**, *254*, 113615. [CrossRef]
43. Simic, M.; Stavrakis, A.K.; Jeoti, V.; Stojanovic, G.M. A Randles Circuit Parameter Estimation of Li-Ion Batteries With Embedded Hardware. *IEEE Trans. Instrum. Meas.* **2022**, *71*, 1004312. [CrossRef]
44. Hassanaly, M.; Weddle, P.J.; King, R.N.; De, S.; Doostan, A.; Randall, C.R.; Dufek, E.J.; Colclasure, A.M.; Smith, K. PINN surrogate of Li-ion battery models for parameter inference, Part II: Regularization and application of the pseudo-2D model. *J. Energy Storage* **2024**, *98*, 113104. [CrossRef]
45. Máthé, L.; Grosu, I. Transport Through a Quantum Dot with Electron-Phonon Interaction. *Mater. Today Proc.* **2018**, *5*, 15878–15887. [CrossRef]
46. Máthé, L.; Grosu, I. Nonequilibrium Kondo effect in a graphene-coupled quantum dot in the presence of a magnetic field. *Beilstein J. Nanotechnol.* **2020**, *11*, 225–239. [CrossRef]
47. Mustafa, H.; Bourelly, C.; Vitelli, M.; Milano, F.; Molinara, M.; Ferrigno, L. SoC estimation on Li-ion batteries: A new EIS-based dataset for data-driven applications. *Data Brief* **2024**, *57*, 110947. [CrossRef]
48. Zhang, S.; Yuan, W.; Wang, Y.; Cheng, S.; Wang, J. Early-stage lifetime prediction for lithium-ion batteries: Linear regression-ensemble learning hybrid model based on impedance spectroscopy geometry. *J. Power Sources* **2024**, *617*, 235153. [CrossRef]
49. Nunes, H.; Martinho, J.; Fermeiro, J.; Pombo, J.; Mariano, S.; Calado, M.D.R. Impedance Analysis and Parameter Estimation of Lithium-Ion Batteries Using the EIS Technique. *IEEE Trans. Ind. Appl.* **2024**, *60*, 5048–5060. [CrossRef]
50. Zhu, H.; Evans, T.A.P.; Weddle, P.J.; Colclasure, A.M.; Chen, B.-R.; Tanim, T.R.; Vincent, T.L.; Kee, R.J. Extracting and Interpreting Electrochemical Impedance Spectra (EIS) from Physics-Based Models of Lithium-Ion Batteries. *J. Electrochem. Soc.* **2024**, *171*, 050512. [CrossRef]
51. Jones, P.K.; Stimming, U.; Lee, A.A. Impedance-based forecasting of lithium-ion battery performance amid uneven usage. *Nat. Commun.* **2022**, *13*, 4806. [CrossRef]
52. Li, C.; Yang, L.; Li, Q.; Zhang, Q.; Zhou, Z.; Meng, Y.; Zhao, X.; Wang, L.; Zhang, S.; Li, Y.; et al. SOH estimation method for lithium-ion batteries based on an improved equivalent circuit model via electrochemical impedance spectroscopy. *J. Energy Storage* **2024**, *86*, 111167. [CrossRef]
53. Júnior, C.A.R.; Sanseverino, E.R.; Gallo, P.; Amaral, M.M.; Koch, D.; Kotak, Y.; Diel, S.; Walter, G.; Schweiger, H.-G.; Zanin, H. Unraveling the degradation mechanisms of lithium-ion batteries. *Energies* **2024**, *17*, 3372. Available online: https://opus4.kobv.de/opus4-haw/frontdoor/index/index/docId/4908 (accessed on 1 December 2024). [CrossRef]

54. Meddings, N.; Heinrich, M.; Overney, F.; Lee, J.-S.; Ruiz, V.; Napolitano, E.; Seitz, S.; Hinds, G.; Raccichini, R.; Gaberšček, M.; et al. Application of electrochemical impedance spectroscopy to commercial Li-ion cells: A review. *J. Power Sources* **2020**, *480*, 228742. [CrossRef]
55. Zhai, N.S.; Li, M.W.; Wang, W.L.; Zhang, D.L.; Xu, D.G. The application of the EIS on Li-ion batteries measurements. *J. Phys. Conf. Ser.* **2006**, *48*, 1157–1161. [CrossRef]
56. Mingant, R.; Bernard, J.; Moynot, V.S.; Delaille, A.; Mailley, S.; Hognon, J.-L.; Huet, F. EIS Measurements for Determining the SoC and SoH of Li-Ion Batteries. *ECS Trans.* **2011**, *33*, 41–53. [CrossRef]
57. Wildfeuer, L.; Gieler, P.; Karger, A. Combining the Distribution of Relaxation Times from EIS and Time-Domain Data for Parameterizing Equivalent Circuit Models of Lithium-Ion Batteries. *Batteries* **2021**, *7*, 52. [CrossRef]
58. Xia, Z.; Abu Qahouq, J.A. Evaluation of Parameter Variations of Equivalent Circuit Model of Lithium-ion Battery under Different SOH Conditions. In Proceedings of the 2020 IEEE Energy Conversion Congress and Exposition (ECCE), Detroit, MI, USA, 11–15 October 2020; pp. 1519–1523.
59. Available online: https://www.dnkpower.com/ncr18650b/ (accessed on 3 December 2024).
60. Available online: https://imrbatteries.com/products/panasonic-ncr18650b-3350mah-4-87a-battery (accessed on 3 December 2024).
61. Available online: https://radenite.com/product.php?prodid=0791126833886 (accessed on 1 December 2024).
62. Available online: https://www.batteryspace.com/prod-specs/ncr18650b.pdf (accessed on 1 December 2024).
63. Available online: https://www.biologic.net/products/vsp-potentiostat/ (accessed on 3 December 2024).
64. Available online: https://mmrc.caltech.edu/BioLogic%20Echem/ECLab%20Manuals/EC-Lab%20software%20Techniques%20and%20Applications%20manual.pdf (accessed on 1 December 2024).
65. Li, Y.; Luo, L.; Zhang, C.; Liu, H. State of Health Assessment for Lithium-Ion Batteries Using Incremental Energy Analysis and Bidirectional Long Short-Term Memory. *World Electr. Veh. J.* **2023**, *14*, 188. [CrossRef]
66. Bruj, O.; Calborean, A. EIS ageing prediction of lithium-ion batteries depending on charge rates. *Batteries* **2024**, *10*, 247. [CrossRef]
67. Liu, Y.; Wu, L. Recent advances of cathode materials for zinc-ion hybrid capacitors. *Nano Energy* **2023**, *109*, 108290. [CrossRef]
68. Available online: https://www.biologic.net/documents/high-precision-coulometry-hpc-battery-application-note-53/ (accessed on 1 December 2024).
69. Available online: http://labman.phys.utk.edu/phys222core/modules/m3/RC%20circuits.html (accessed on 1 December 2024).
70. Available online: https://www.bbc.co.uk/bitesize/guides/zbf6cqt/revision/1 (accessed on 1 December 2024).
71. Available online: https://physics.info/electric-power/summary.shtml (accessed on 1 December 2024).
72. Available online: https://eng.libretexts.org/Courses/Oxnard_College/Matlab_and_Octave_Programming_for_STEM_Applications_(Smith)/10:__Interpolation_and_Curve_Fitting/10.02:_Nonlinear_Interpolation (accessed on 1 December 2024).